catalysts

MDPI

Article

Highly Selective pH-Dependent Ozonation of Cyclohexane over Mn/γ-Al_2O_3 Catalysts at Ambient Reaction Conditions

Siphumelele Thandokwazi Mkhondwane and Viswanadha Srirama Rajasekhar Pullabhotla *

Department of Chemistry, University of Zululand, Private Bag X1001, Kwa-Dlangezwa 3886, South Africa; siphumelele2004@gmail.com

* Correspondence: PullabhotlaV@unizulu.ac.za; Tel.: + 27-35-902-6155

Received: 28 September 2019; Accepted: 28 October 2019; Published: 15 November 2019

Abstract: The selective oxidation of cyclohexane to a mixture of cyclohexanol and cyclohexanone (KA oil) is one of the imperative reactions in industrial processes. In this study, the catalytic performance of manganese-supported gamma alumina (Mn/γ-Al_2O_3) catalysts is investigated in the selective oxidation of cyclohexane at ambient conditions using ozone. The catalysts were prepared by the wet impregnation method, and their physio-chemical properties were studied by Fourier Transform Infrared (FT-IR) spectroscopy, X-ray diffraction (XRD) spectroscopy, Scanning Electron Microscopy-Energy Dispersive X-ray spectroscopy (SEM-EDX), Transmission Electron Microscopy (TEM), Inductively Coupled Plasma (ICP) spectroscopy, and Brunauer Emmett and Teller (BET). The reaction conditions were optimised considering various parameters such as reaction time, pH, and various percentages of the manganese supported in gamma alumina. The oxidation of cyclohexane was conducted in an impinger reactor unit at pH 3, 7, and 11 for 1 h of ozonation time. The aliquots were collected after 30 min and 1 h of ozonation time and analysed with GC-MS and FT-IR spectroscopy. The 2.5% Mn/γ-Al_2O_3 catalyst exhibited a significantly enhanced catalytic performance at pH 3 and 7 with a percentage conversion of 9% and 15% at pH 3 and 7, respectively, after 30 min of ozonation time. However, after 1 h of ozonation time, the percentage conversions were increased to 23% and 29% at pH 3 and 7, respectively. At pH 11, 5% Mn/γ-Al_2O_3 exhibit high catalytic performance with a percentage conversion of 19% and 31% after 30 minutes and 1 h of ozonation time, respectively. The percentage selectivity obtained is 100% toward KA oil and/or cyclohexanone depending on pH and reaction time.

Keywords: oxidation; Mn/γ-Al_2O_3 catalyst; ozone; cyclohexane and KA oil

1. Introduction

The functionalisation of the saturated aromatic and aliphatic hydrocarbon's C-H bond is one of the utmost important industrial processes in the quest for economic viability and a sustainable approach for the production of oxygenates. However, the C-H bond is very stable toward different oxidants and, therefore, it requires extreme reaction conditions, such as high temperature and pressure. Moreover, the corresponding oxygenates are more reactive than their respective parent hydrocarbons, and as a result, they subsequently react to form un-wanted products [1]. One of such processes is the oxidation of cyclohexane, which has shown increasing importance for the production of cyclohexanol and cyclohexanone (a mixture called KA oil). The constituents of KA oil are prominent intermediates for the production of caprolactam and adipic acid. Caprolactam and adipic acid are important precursors for the production of nylon 6 and nylon 6,6 polymers, respectively [2–4].

The production of KA oil at an industrial scale employs the oxidation of cyclohexane at 150–160 °C and 1–2 atm of temperature and pressure conditions, respectively, using sodium boric acid and

manganese salts as homogenous catalysts. In this process, the percentage conversion obtained for cyclohexane oxidation was 4% to 6%. These conditions were applied to avoid further oxidation of the reaction product (cyclohexanol and cyclohexanone). The percentage selectivity obtained was as high as 70%–80% [5,6]. However, the homogenous catalysts are associated with several drawbacks, such as the instability at high temperatures, difficulty in separating the catalysts from the reaction mixture, and the need for the disposal of waste [7]. Furthermore, the use of high temperature and pressure conditions has been the major safety concern ever since the cyclohexane reactor explosion, which occurred in the Flixborough village on 1 June 1974 that caused 28 casualties [8,9]. These stumbling blocks address the need for an agent establishment of the efficient cyclohexane oxidation process.

In recent years, the concept of ozone-initiated catalytic oxidation has been a promising platform for the efficient, selective, and environmental benign contemporary transformation of hydrocarbons [10–12]. The utilisation of ozone in the course catalytic oxidation processes helps in decreasing activation energy when compared to other oxidants such as oxygen, hydrogen peroxide, and tert-butyl hydrogen peroxide [13,14]. Ozone is a strong oxidising agent, which is commonly used for oxidative degradation of organic compounds to value-added products [15]. Ozone offers numerous advantages in oxidation processes compared to other oxidants, such as mineralisation rate, short reaction duration, higher oxidation potential (2.07 V) than the other oxidising agents such as permanganate (1.67 V), chlorine dioxide (1.57 V), hypochlorous acid (1.49 V), chlorine (1.36 V), hypobromous acid (1.33 V), and oxygen (1.23 V), and enhanced efficiency [16,17]. Most commonly, ozone-related oxidation processes entail the transformation of the ozone into highly reactive secondary species, such as hydroperoxyl and hydroxyl radicals via decomposition for optimum efficiency [18]. This is usually achieved by utilising heterogeneous catalysts such as Ni, Mn, and Co. Mehandjiev et al. has pointed manganese to be of the highest activity in ozone decomposition among other p-type transition metals [19–21]. In this case, the decomposition of ozone on the Mn surface produces hydroxyl radicals, which subsequently play a part in the oxidation reaction of the hydrocarbons [22,23]. However, due to the stability differences between cyclohexane and the corresponding oxygenates (KA oil), not much has been reported on catalytic oxidation of cyclohexane using ozone ("catazone"). This is because oxygenates are further oxidised to form unwanted products. However, most of these studies are conducted under extreme reaction conditions.

In the current study, we report the catalytic ozonation of cyclohexane over Mn/γ-Al_2O_3 catalysts using ozone. Gamma alumina was selected as the support because of its mechanical strength and high surface-to-volume ratio [21]. On the other hand, manganese is suitable for oxidation of cyclohexane owing to its facile redox behaviour, which facilitates oxygen diffusion and high oxygen adsorption capacity.

2. Results and Discussion

2.1. Catalysts Characterisation

2.1.1. Fourier Transform Infrared (FT-IR) Spectroscopy

Figure 1 depicts the FT-IR spectra of gamma alumina (γ-Al_2O_3) support and various percentages of manganese-supported gamma alumina (Mn/γ-Al_2O_3) catalysts. The broad band is observed in the FT-IR spectra of γ-Al_2O_3 support and all the as-synthesised Mn/γ-Al_2O_3 catalysts at a wavelength of 3500 cm^{-1}, which becomes more perceptive with an increase in metal loading. This band is indexed to the vibrational stretching frequency of the hydroxyl (O-H) groups present on Lewis acid sites of γ-Al_2O_3 and Mn/γ-Al_2O_3 catalysts that resulted from adsorbed water molecules. Furthermore, Figure 1 also shows a weak absorption band at 1600 cm^{-1}, which could be indexed to the asymmetric stretching vibrations of Al-OH [24,25].

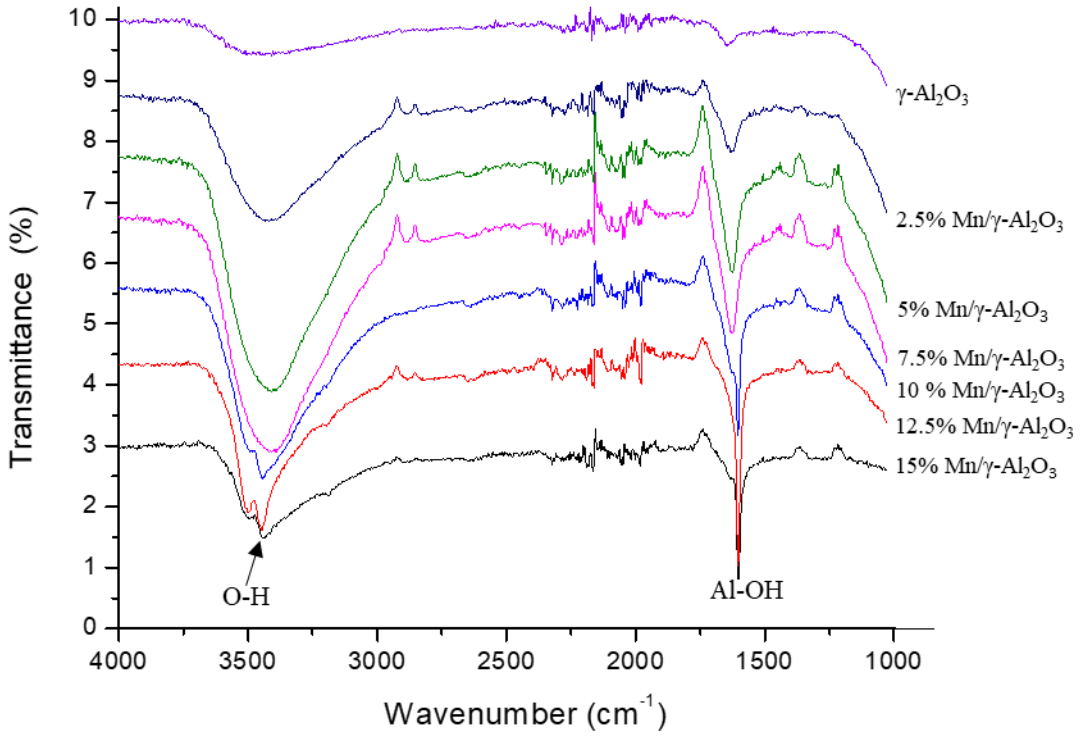

Figure 1. FT-IR spectra of γ-Al_2O_3 and various percentages of Mn/γ-Al_2O_3 catalysts.

2.1.2. X-Ray Diffraction

The X-ray diffractograms of gamma alumina (γ-Al_2O_3) support, and various percentage manganese-supported gamma alumina (Mn/γ-Al_2O_3) catalysts are shown in Figure 2. The characteristic peaks observed at $2\theta = 37.7°$, 45.9°, and 67° refer to (331), (222), and (440) miller indices, which are indexed to γ-Al_2O_3 support [26] cubic structure as confirmed by JCPDS card 1839-28. The XRD of γ-Al_2O_3 exhibit characteristic peaks of a highly crystalline material. However, the incorporation of the manganese results in crystal imperfection and a decrease in particle size of the γ-Al_2O_3 support, observed by a significant degree of peak broadness in all X-ray diffraction peaks corresponding to γ-Al_2O_3. This was also reported by Maldonado et al., for the incorporation of Fe in γ-Al_2O_3 [27]. Furthermore, the incorporation of Mn also results in a disappearance of the diffraction peaks corresponding to (101) and (111) miller indices at $2\theta = 16.87°$ and 20.43°, respectively. The existence of Mn in 2.5%, 5%, 7.5%, and 10% Mn/γ-Al_2O_3 catalysts is trivial as there are no visible diffraction peaks corresponding to Mn. This suggests that Mn is well incorporated at the nano-sized scale of γ-Al_2O_3 support. Small diffraction peaks attributed to the MnO phase are observed at $2\theta = 17.24°$, 20.43°, 31.62°, and 43.5° with (200), (111), (311), and (112) miller indices in 12.5% and 15% Mn/γ-Al_2O_3. There are no other manganese phases observed other than the MnO observed in the 12.5% and 15% Mn/γ-Al_2O_3 catalysts.

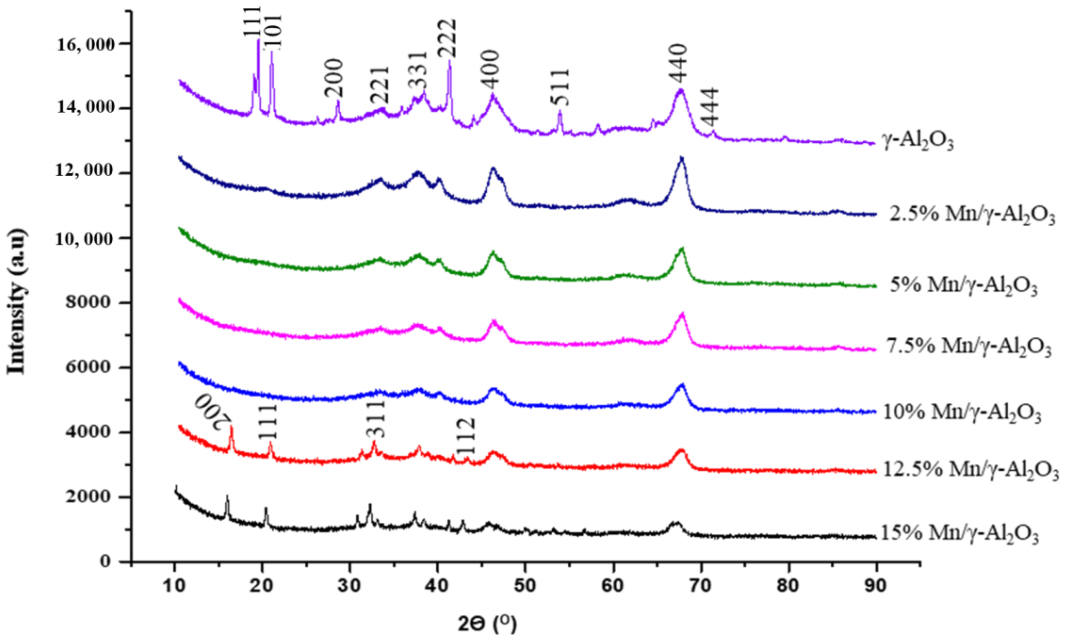

Figure 2. XRD patterns of γ-Al_2O_3 and various percentages of Mn/γ-Al_2O_3 catalysts.

2.1.3. Scanning Electron Microscopy (SEM)

Figure 3a–d displays SEM images of γ-Al_2O_3 and various percentages of Mn/γ-Al_2O_3 catalysts. The γ-Al_2O_3 support appears as fluffy particles with poorly defined structure. The morphology displays a rough surface with high surface defects. However, upon Mn loading, the surface becomes fine and aggregated. This can be clearly observed with the increase in Mn content. The existence of Manganese particles was further confirmed by Energy Dispersive X-ray spectroscopy (EDX) images shown in Figure S3a–f.

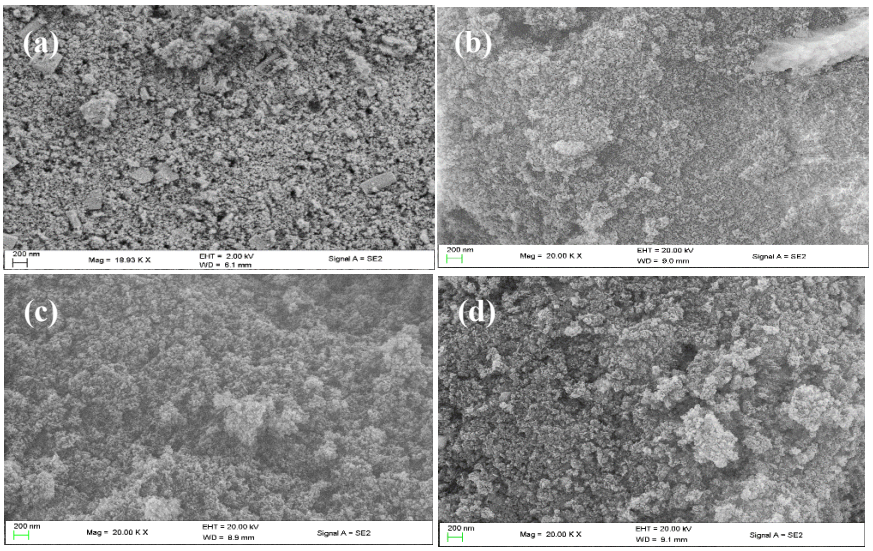

Figure 3. SEM images of (**a**) γ-Al_2O_3, (**b**) 2.5% Mn/γ-Al_2O_3, (**c**) 5% Mn/γ-Al_2O_3, (**d**) 7.5% Mn/γ-Al_2O_3 catalysts.

2.1.4. Transmission Electron Microscopy (TEM)

TEM images of γ-Al_2O_3 support, and various percentages of Mn/γ-Al_2O_3 catalysts, are depicted in Figure 4. The γ-Al_2O_3 display spherical shaped particles with uniform particle size (13 nm). However,

the incorporation of Mn is accompanied by the significant decrease in particle size and shape from spherical to rod shape, which is observed in all Mn/γ-Al_2O_3 catalysts. The decrease in the particle size displayed by TEM results is in good agreement with the XRD results and it becomes more perceptive with an increase in manganese loading from 10%–15% Mn/γ-Al_2O_3 catalysts (Figure S2, supplementary data). The particle size and length of the Mn/γ-Al_2O_3 catalysts is between 7–9 nm and 16–23 nm, respectively. The variation in particle shape of γ-Al_2O_3 and Mn/γ-Al_2O_3 is attributed to the elongation and agglomeration of some particles.

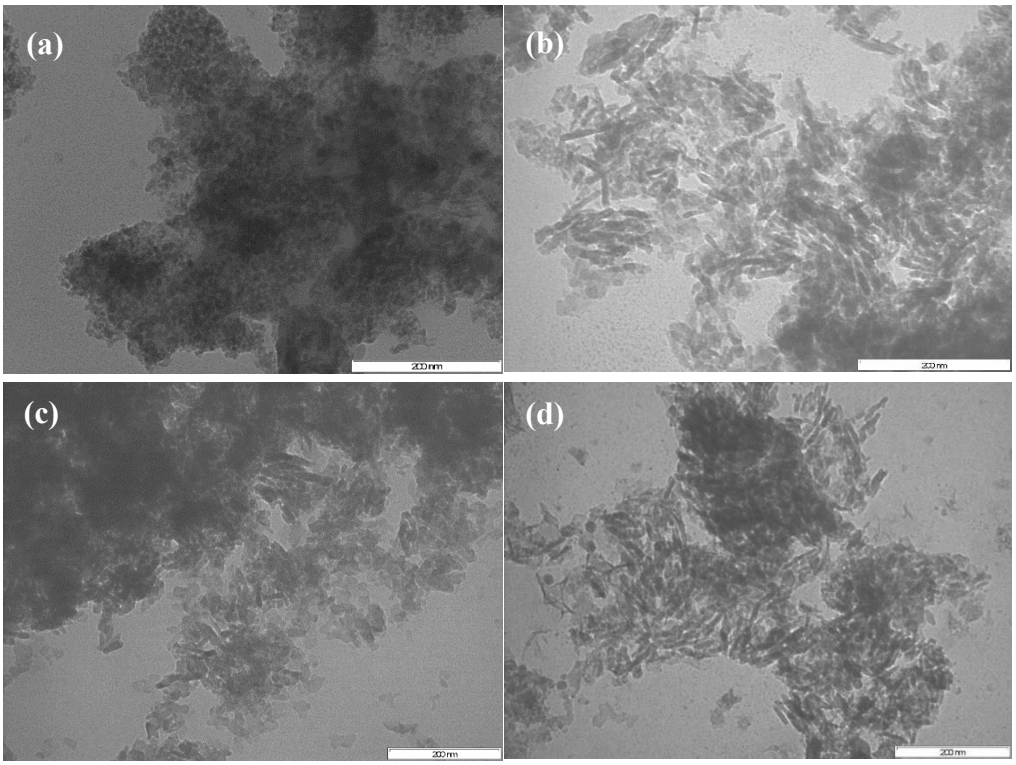

Figure 4. TEM images of (**a**) γ-Al_2O_3 support, (**b**) 2.5% Mn/γ-Al_2O_3, (**c**) 5% Mn/γ-Al_2O_3, (**d**) 7.5% Mn/γ-Al_2O_3 catalysts.

2.1.5. Inductively Coupled Plasma (ICP) and Energy Dispersed X-Ray (EDX) Spectroscopy

The theoretical and experimental weight percentage of manganese loaded γ-Al_2O_3 catalysts obtained from ICP and EDX spectroscopy is presented in Table 1. The experimental Mn percentage is very close to the anticipated theoretical percentage from the results obtained using both ICP and EDX spectroscopy (Figure S3a–f, supplementary data), which suggest that manganese was successfully incorporated into the γ-Al_2O_3 support.

Table 1. Inductively coupled plasma (ICP) and energy dispersed X-Ray spectroscopy (EDX) results of Mn/γ-Al_2O_3 catalysts.

Catalyst	Theoretical Mn wt %	ICP Mn wt %	EDX Mn wt% *
2.5% Mn/γ-Al_2O_3	2.50	2.48	2.33
5% Mn/γ-Al_2O_3	5.00	5.39	5.9
7.5 % Mn/γ-Al_2O_3	7.50	7.46	7.57
10% Mn/γ-Al_2O_3	10.0	9.18	10.23
12.5% Mn/γ-Al_2O_3	12.5	12.48	12.42
15% Mn/γ-Al_2O_3	15.0	14.94	15.64

* Figure S3a–f, supplementary data.

2.1.6. Brunauer-Emmet-Teller (BET) Surface Area

Table 2 displays the BET results for pure γ-Al_2O_3 support, 2.5% and 7.5% Mn/γ-Al_2O_3. The surface area of γ-Al_2O_3 is 295.0 m^2/g. However, the surface areas of 2.5 and 7.5 % Mn/γ-Al_2O_3 are 167.6 and 107.8 m^2/g, respectively, which are lower than that obtained from γ-Al_2O_3. Furthermore, the pore volumes of 2.5% and 7.5% Mn/γ-Al_2O_3 are 0.3827 and 0.3022 cm^3/g, respectively. The incorporation of Mn in the γ-Al_2O_3 support results in the decrease in both surface area and pore volume. This becomes more significant with increasing Mn content. This is caused by pores that are filled and blocked by Mn particles, which results in an increased surface area of the Mn/γ-Al_2O_3 catalysts. However, the further increase of the Mn content results in poor synergic interaction between Mn and γ-Al_2O_3.

Table 2. Brunauer-Emmet-Teller (BET) surface areas of γ-Al_2O_3, 2.5% and 7.5% Mn/γ-Al_2O_3 catalysts.

Catalysts	BET Surface Area (m^2/g)	Pore Volume (cm^3/g)	Pore Size (nm)
γ-Al_2O_3	295.0	-	-
2.5% Mn/γ-Al_2O_3	167.6	0.3827	9.13
7.5% Mn/γ-Al_2O_3	107.8	0.3022	11.21

2.2. Characterisation of the Reaction Mixture

Gas Chromatography-Mass Spectrometry (GC-MS) and Fourier Transform Infrared (FT-IR) Spectroscopy: The gas chromatography results obtained (Figure 5) display three significant chromatographic peaks for the reaction mixture sample drawn after 30 min of ozonation time, which corresponds to cyclohexane (3.4 min retention time), cyclohexanol (6.6 min retention time), and cyclohexanone (6.8 min retention time). However, only two chromatographic peaks were observed in the reaction mixture sample drawn after 1 h ozonation, corresponding to cyclohexane and cyclohexanone at pH 3 and 7. Whereas, at pH 11 for both the samples drawn at 30 min and 1 h of ozonation time, three chromatographic peaks corresponding to cyclohexane, cyclohexanol, and cyclohexanone were observed. The mass-spectrometry results further confirmed the identified ozonation products (Figures S4–S6). Gas chromatogram of cyclohexane and its mass spectrum with molecular ion peaks (m/z = 84, 56, and 29) before ozonation are represented in Figure S4 (supplementary data). Gas chromatogram of ozonated cyclohexane after 30 min and its mass spectra for cyclohexane with molecular ion peaks (m/z = 84, 56, and 29), cyclohexanol with molecular ion peaks (m/z = 82, 57, 29) and cyclohexanone with molecular ion peaks (m/z = 98, 55, 27) are demonstrated in Figure S5 (supplementary data). Gas chromatogram of ozonated cyclohexane after 1 h and its mass spectra for cyclohexane with molecular ion peaks (m/z = 84, 56, and 29) and cyclohexanone with molecular ion peaks (m/z = 98, 55, 27) are displayed in Figure S6 (supplementary data). From Figure S6, it is evident that the cyclohexanol formed during the first 30 min of the reaction got further oxidised to cyclohexanone.

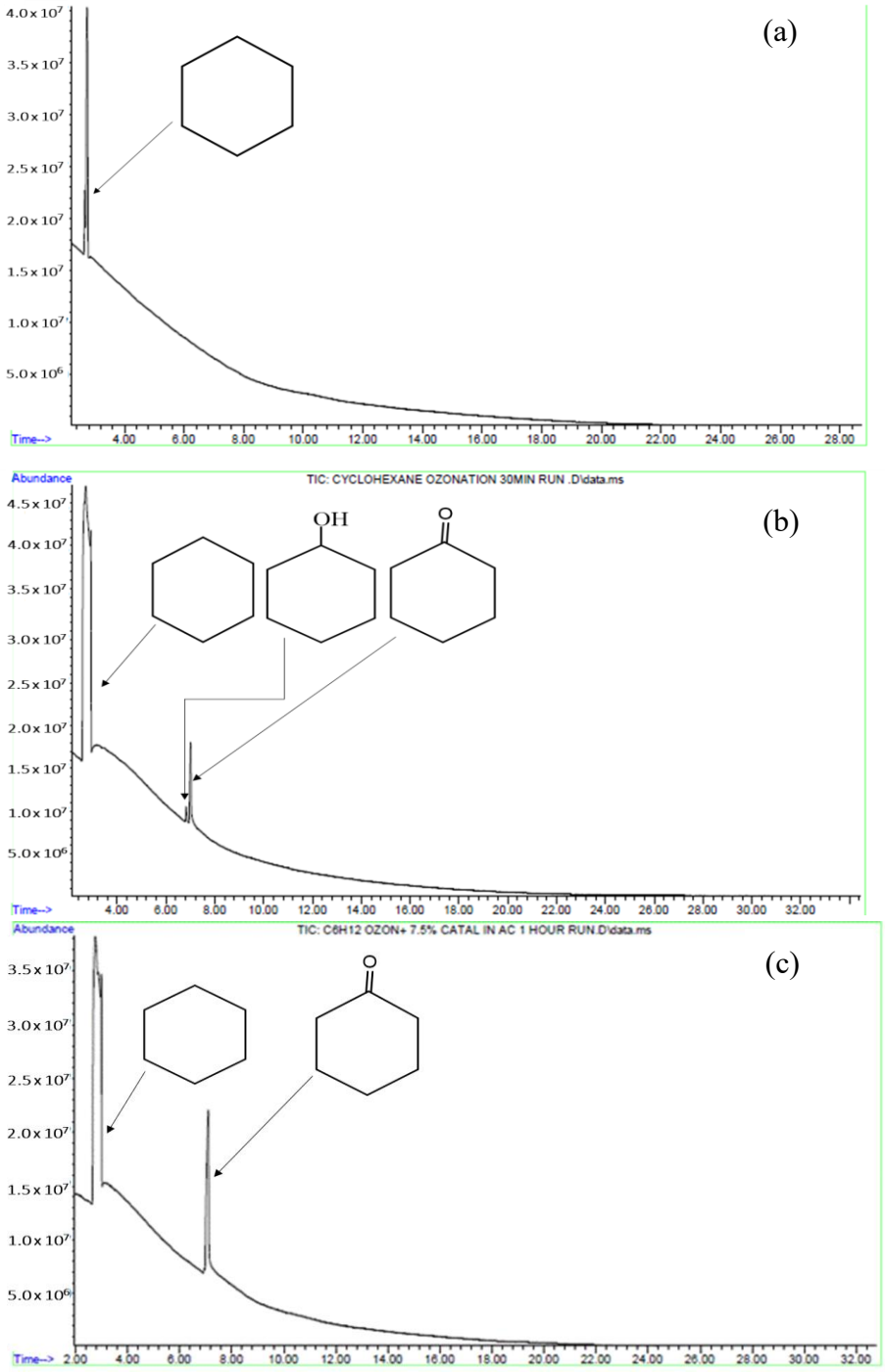

Figure 5. Gas chromatograms of the 2.5% Mn/γ-Al_2O_3 catalysed cyclohexane oxidation mixtures (**a**) before ozonation, (**b**) after 30 min ozonation, and (**c**) after 1 h ozonation time at ambient conditions and pH = 3.

FT-IR spectra in Figure 6 displays both hydroxyl (3500 cm^{-1}) and carbonyl (1717 cm^{-1}) groups for the reaction mixture samples drawn after 30 min of ozonation time at pH 3, 7, and 11, corresponding to cyclohexanol and cyclohexanone (1717 cm^{-1}), as identified by GC-MS. From the 1 h ozonated reaction mixture samples, only the carbonyl group was observed. Furthermore, at pH 11, hydroxyl and carbonyl groups were observed for both the reaction mixture samples drawn after 30 min and 1 h of ozonation time. This is in good agreement with the GC-MS results.

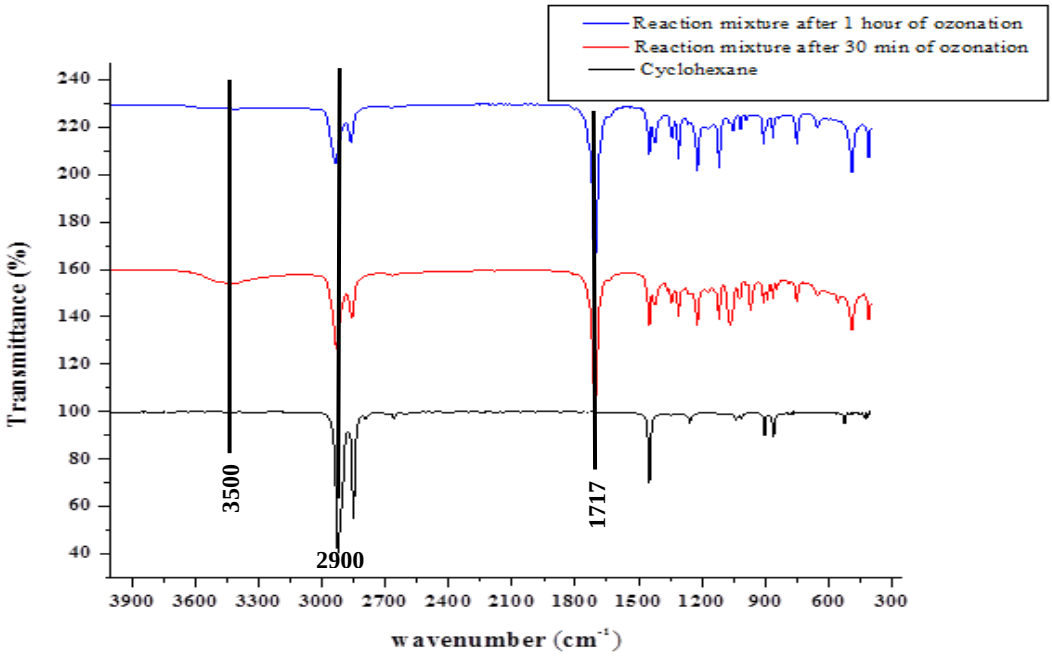

Figure 6. FT-IR spectra of 2.5% Mn/γ-Al_2O_3 catalysed cyclohexane oxidation mixture at ambient reaction conditions and pH = 3 drawn after 30 min and 1 h of ozonation.

2.3. Oxidation of Cyclohexane

2.3.1. Percentage Conversion

Figure 8a,b and Table 3 summarise the catalytic performance of the Mn/γ-Al_2O_3 catalysts in terms of the percentage conversion in the ozone initiated oxidation of cyclohexane at pH 3, 7, and 11 (samples were drawn after 30 min and 1 h of ozonation time); at 20 °C and 1 atm conditions. For comparison purposes, blank and γ-Al_2O_3 catalysed ozonation reactions were initially performed, followed by the Mn/γ-Al_2O_3 catalysed ozonation reactions. It can be seen from Figure 7a,b and Table 3 that in the absence of any catalyst and in the presence of γ-Al_2O_3 (support only) the percentage conversion is relatively low. The percentage conversion of cyclohexane in the absence of the catalyst is 4, 6 and 9% at pH 3, 7, and 11, respectively, for the samples drawn after 30 min of ozonation time. However, after 1 h of ozonation time, the conversion is 9%, 12% and 16% at pH 3, 7, and 11, respectively. On the other hand, γ-Al_2O_3 showed poor catalytic activity in terms of percentage conversion, and the results observed were slightly higher than that of blank ozonation. However, these percentage conversions appear lower when the Mn/γ-Al_2O_3 catalysts were employed in the cyclohexane oxidation reaction. The Mn/γ-Al_2O_3 catalysts exhibit high catalytic performance at pH 3 and 7, with percentage conversion of 9% and 15% for the reaction mixture drawn after 30 minutes of ozonation time. With 1 h ozonation samples, the percentage conversion obtained was 23% and 28% at pH 3 and 7, respectively. At pH 11, 2.5% Mn/γ-Al_2O_3 catalyst exhibited high catalytic performance with a percentage conversion of 23% and 31% (for samples drawn after 30 minutes and 1 h of ozonation time), respectively.

From these results, it can be postulated that the high catalytic performance of the Mn/γ-Al_2O_3 catalyst is attributed to the incorporation of manganese into γ-Al_2O_3. The optimum catalytic performance of Mn/γ-Al_2O_3, in terms of percentage conversion, results from a vast number of factors. For example, in comparison with γ-Al_2O_3, the XRD results exhibit a decreased particle size and crystal stability of the Mn/γ-Al_2O_3 catalyst. The decrease in particle size results into an increase in surface area, and therefore, a more active site available to the substrate. The decrease in particle size is typical for metal-supported catalysts [28]. Similarly, the TEM results confirm the decrease in particle size of the Mn/γ-Al_2O_3 catalyst and further reveal the change in particle shape from spherical to rod-shaped particles when compared with that of γ-Al_2O_3. The rod-shaped particles also provide high surface

area compared to spherical shaped particles [29]. In addition, the high catalytic performance of the Mn/γ-Al_2O_3 catalysts can also be explained by aspects of the metal-support relationship of the metal-supported catalysts [28,30–32]. That is, the γ-Al_2O_3 support stabilises the MnO nanoparticles through electron transfer between the support and the metal. In this manner, the surface charge (superoxide) of the Mn is induced. Consequently, the surface charge either directly participates in C-H bond activation via hydrogen abstraction or induces surface hydroxide species through dissociative adsorption of water molecules [33]. The hydroxide species decomposes ozone to form a hydroxide radical and subsequently, the hydroxide radical [34]. The existence of the hydroxyl species is evidenced in the FT-IR results of the Mn/γ-Al_2O_3 catalysts. The catalytic performance of the Mn/γ-Al_2O_3 catalysts gradually decreased with an increase in percentage of Mn incorporation into γ-Al_2O_3. This is common for metal-supported catalysts. This is probably caused by the blockage of the γ-Al_2O_3 pores by excess Mn, therefore limiting cyclohexane diffusion into the active sites inside the pore. This is in good agreement with the BET results of the 2.5% and 7.5% Mn/γ-Al_2O_3 catalysts shown in table 2, in which the pore volume decreases with increasing Mn content.

Table 3. Cyclohexane percentage conversion and selectivity toward KA oil at 20 ± 1 °C and 1 atm.

Catalyst	Reaction Time	Conversion (%)			Selectivity (%)					
					Cyclohexanol			Cyclohexanone		
		pH 3	pH 7	pH 11	pH 3	pH 7	pH 11	pH 3	pH 7	pH 11
Blank ozonation	30 min	3	6	9	9	12	14	91	88	86
	1 h	9	12	16	-----	-----	2	100	100	98
γ-Al_2O_3	30 min	7	9	11	8	10	11	92	90	89
	1 h	11	13	19	-----	-----	6	100	100	94
2.5% Mn/γ-Al_2O_3	30 min	9	15	17	6	7	15	94	93	95
	1 h	23	29	28	-----	-----	3	100	100	97
5% Mn/γ-Al_2O_3	30 min	7	11	23	4	8	7	86	92	93
	1 h	19	21	31	-----	-----	7	100	100	93
7.5% Mn/γ-Al_2O_3	30 min	9	8	19	7	13	13	93	87	87
	1 h	17	19	28	-----	-----	5	100	100	95
10% Mn/γ-Al_2O_3	30 min	6	9	16	8	10	6	92	90	94
	1 h	14	18	24	-----	-----	2	100	100	98
12.5% Mn/γ-Al_2O_3	30 min	8	11	14	2	6	9	98	94	91
	1 h	12	18	20	-----	-----	8	100	100	92
15% Mn/γ-Al_2O_3	30 min	5	7	15	12	8	11	88	92	89
	1 h	11	14	17	-----	-----	4	100	100	96

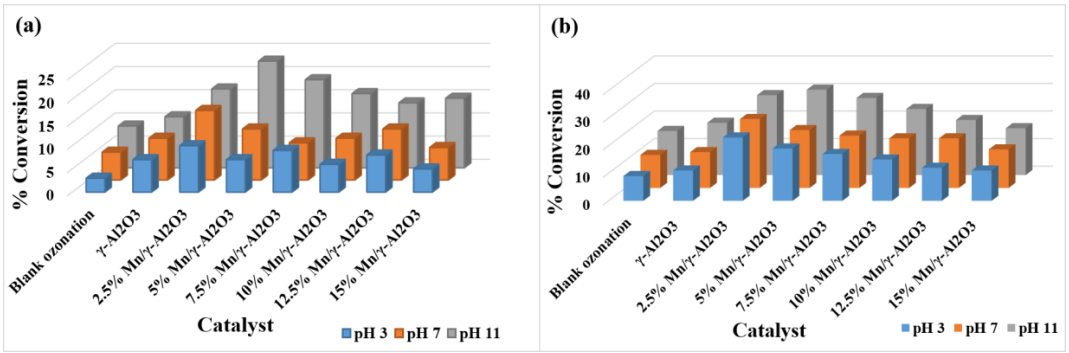

Figure 7. Percentage conversion profiles of cyclohexane vs. catalysts after (**a**) 30 min and (**b**) 1 h of ozonation time at 20 ± 1 °C and 1 atm.

2.3.2. Percentage Selectivity

Table 3 and Figure 8a–c display the percentage selectivity plot of cyclohexane oxidation at pH 3, 7, and 11 after 30 min and 1 h of reaction time. Theoretically, the oxidation of cyclohexane is anticipated

to selectively result in the mixture of cyclohexanol and cyclohexanone and other by-products, such as cyclohexyl hydroperoxide, hexanolactone, adipic acid, and ester dicyclohexyl adipate [7,20]. Contrarily, from the percentage selectivity plot in Figure 8a–c and Table 3, it can be noted that the current study was solely selective to either both cyclohexanol and cyclohexanone and/or cyclohexanone. Nevertheless, most cyclohexane oxidation studies have been conducted at high temperatures and pressure conditions to enhance percentage conversion [1,2,7,20]. High temperature and pressure conditions are highly vigorous and advance the production of the radicals, which subsequently react with cyclohexanol and cyclohexanone to produce undesired products. This is mainly because cyclohexanol and cyclohexanone are more reactive than cyclohexane, and therefore, when available, they can be easily oxidised to hexanolactone, adipic acid, dicylcohexyl adipate, and the ester more rapidly. With that being said, the current study opted for ambient temperature (20 ± 1 °C) and pressure (1 atm) conditions, therefore, limiting the production of the radicals. As a result, the 100% selectivity toward the desired products (mixture of cyclohexanol and cyclohexanone) is obtained, which has never been reported before. The overall percentage selectivity range toward cyclohexanol and cyclohexanone was 2%–12% and 88%–98% at pH 3, 6%–13% and 87%–94% at pH 7, and 9%–22% and 78%–91% at pH 11, respectively, after 30 min of ozonation time. After 1 h of ozonation time, the percentage selectivity was 100% toward cyclohexanone at pH 3 and 7. However, at pH 11, the overall percentage selectivity range was 3%–7% and 93%–97% toward cyclohexanol and cyclohexanone, respectively. This suggests that cyclohexane is first converted to cyclohexanol and then further oxidised to cyclohexanone. This is in good agreement with the literature [29].

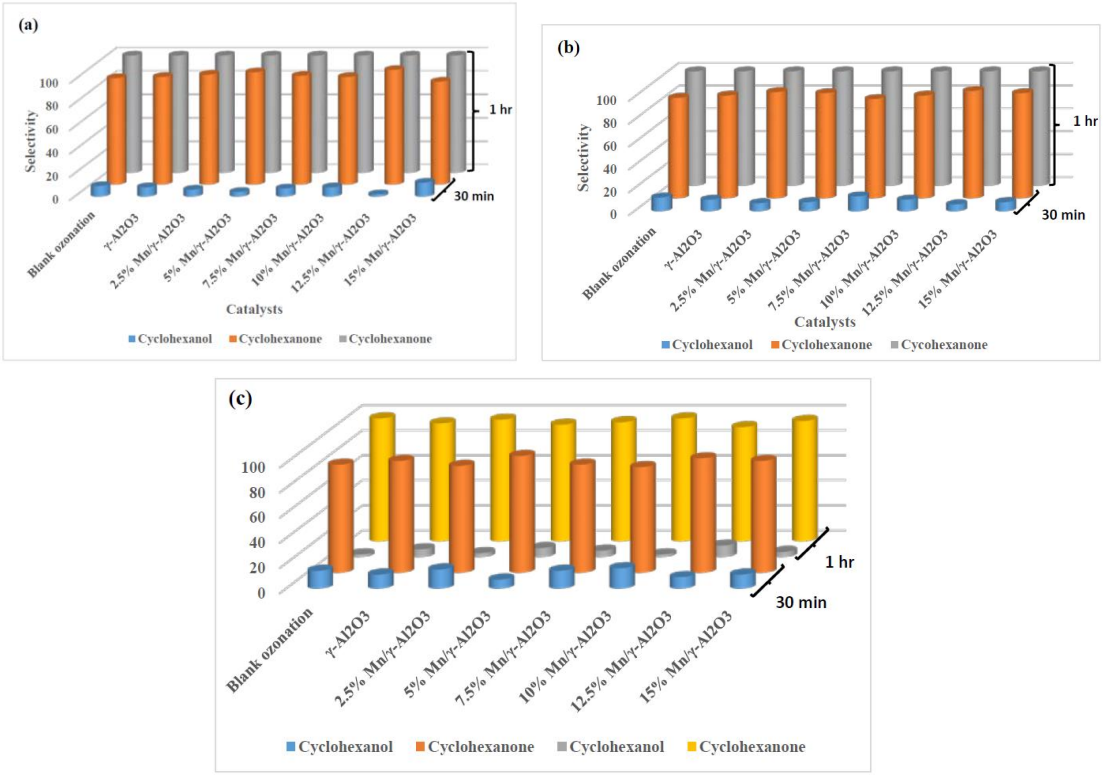

Figure 8. Percentage selectivity profiles of cyclohexane vs. catalysts at (**a**) pH 3, (**b**) pH 7, and (**c**) pH 11 after 30 min and 1 h of ozonation time at 20 ± 1 °C and 1 atm.

2.3.3. The Effects of the pH

From the results displayed in Table 3 and Figures 7 and 8, it can be seen that pH is one of the uppermost important parameters affecting percentage conversion and selectivity in the cyclohexane ozonation. The percentage conversion increases with an increase in pH from pH = 3, 7, and 11 for

both blank ozonation and the catalysed ozonation reactions. Furthermore, the selectivity toward cyclohexanol gradually increases with an increase in pH from pH = 3, 7, and 11 for both 30 min and 1 h of ozonation time. However, selectivity toward cyclohexanone decreases with an increase in pH from pH= 3, 7, and 11. This is mainly because the pH substantially controls the decomposition pathway of ozone. At acidic conditions, the proton readily reacts with ozone to form molecular oxygen (O_2) and water (H_2O) (Equation (1)). However, under basic conditions, the hydroxide ion (OH^-) reacts with ozone (O_3) to form a hydroxyl radical (Equation (2)), which is more reactive than ozone and oxygen. Therefore, the hydroxyl radical provides higher oxidation potential than ozone and oxygen [34].

$$\text{Acidic conditions: } O_3 + 2H^+ + 2e^- \rightarrow O_2 + H_2O \quad (1)$$

$$\text{Basic conditions: } O_3 + OH^- \rightarrow O_3^{\bullet} + OH^{\bullet} \quad (2)$$

In order to rationalize the effect of the reaction pH in both percentage conversion and selectivity, it is of crucial importance to consider the general free radical chain reaction mechanism proposed for the cyclohexane oxidation reactions [29,31,32]. The initial step of the oxidation involves C-H bond activation via hydrogen atom abstraction from cyclohexane to form cyclohexyl radical (i). This occurs by a number of events, such as: (1) the H-abstraction by an oxidant, (2) H-abstraction by the radical species present in a solution, (3) the cleavage by the unsaturated metal centre, and (4) H-abstraction by the superoxide oxide species bound to metal oxide or the metal centre [34]. The proposed mechanism for the ozone-initiated oxidation of the cyclohexane is shown in Scheme 1. In general, the ozonation of cyclohexane in the absence of the catalyst is initiated by cyclohexane H-abstraction by the ozone-producing cyclohexyl radical and hydrogen trioxide radical (i) [33–35]. Subsequently, hydrogen trioxide radical dissociates to the oxygen and hydroxide radical (ii) [35]. The hydroxide radical reacts with the cyclohexyl radical to form the cyclohexanol (iii) [34]. Ozone further abstracts the hydrogen atom from cyclohexanol to form cyclohexyl hydrogen monoxide radical and hydrogen trioxide radical (iv). The hydrogen trioxide radical dissociates into oxygen and hydroxide radical (ii) [35,36], which subsequently react with cyclohexyl hydrogen monoxide to form cyclohexyl diol. The cyclohexyl diol upon dehydration produces cyclohexanone (v) [33].

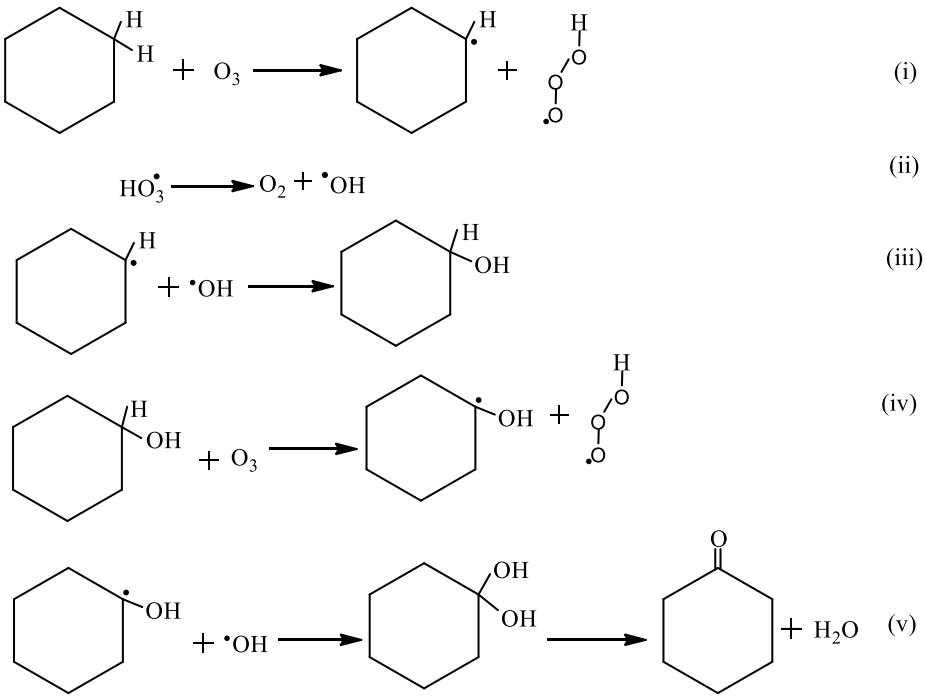

Scheme 1. Ozone initiated oxidation of cyclohexane mechanism.

Based on the reaction shown in Equation (1), the oxidation of cyclohexane under acidic conditions proceeds through C-H bond activation by H-abstraction by oxygen to form a cyclohexyl radical and hydrogen peroxide radical. Since the oxygen molecule is less reactive than ozone, the rate of the cyclohexane H-abstraction in acid medium is slower than under neutral conditions [20]. Consequently, oxygen reacts with the cyclohexyl radical to form the cyclohexyl peroxide radical, which redly abstract the hydrogen atom from cyclohexane to form cyclohexyl hydrogen peroxide. The formation of cyclohexanol proceeds through the decomposition of cyclohexyl hydrogen peroxide [33]. However, under basic conditions, the H-abstraction is promoted by the hydroxide radical from ozone decomposition to form a cyclohexyl radical and water molecule [34]. Ultimately, cyclohexanol is formed from the reaction between the cyclohexyl radical and hydroxide radical [29,33]. Therefore, cyclohexane oxidation at high pH is dominated by rapid production of cyclohexanol. This justifies the high cyclohexanol product selectivity obtained at pH =11 in this study when compared to pH = 3 and pH = 7.

3. Materials and Methods

Cyclohexane (99.99%, Aldrich, St. Louis, MO, Germany), manganese chloride tetrahydrate (98%, Aldrich, St. Louis, MO, Germany), gamma alumina nano-powder (99.99%, Aldrich, St. Louis, MO, Germany), Acetic acid (99.8%, Merck, Gauteng, 1645, South Africa), Sodium hydroxide (99.99%, Merck, Gauteng, 1645, South Africa), hydrofluoric acid (40%, Merck, Gauteng, 1645, South Africa), nitric acid (45%, Merck, Gauteng, 1645, South Africa), toluene (98% Merck, Gauteng, 1645, South Africa), and hydrochloric acid (37%, Merck, Gauteng, 1645, South Africa) were purchased and used without further purification.

3.1. Catalyst Preparation

The catalysts (2.5%, 5%, 7.5%, 10%, 12.5%, and 15% Mn/γ-Al_2O_3) were prepared using the wet impregnation method. The amount of the $MnCl_2.4H_2O$ dissolved in 100 mL of distilled water was calculated based on the percentage of manganese supported in γ-Al_2O_3. In a typical method, an adequate amount of manganese chloride tetrahydrate ($MnCl_2.4H_2O$) was dissolved in 100 mL of distilled water. The resultant solution was slowly (dropwise) dispensed into a 250 mL beaker containing bare γ-Al_2O_3 nano-powder supported with vigorous stirring for homogenous dispersion of Mn into γ-Al_2O_3. Consequently, water was evaporated by placing the beaker on a hot plate at 70 °C for 2 h until a thick paste was obtained. The evaporation of water was completed by drying the catalyst precursor at 90 °C in an oven overnight under oxygen flow followed by calcination at 300 °C for 5 h [37].

3.2. Catalyst Characterisation

FT-IR spectroscopy analysis was performed with a Bruker Tensor 27 FT-IR spectrometer (Bruker, Gauteng, South Africa) with a standard ATR cell. Ethanol was used to clean the surface of the cell prior to every analysis. The pressure was adjusted to 90 gauge for proper contact between the surfaces.

The powder X-ray diffraction (XRD) analysis was performed using Bruker AXS-D8 diffractometer with a CuKα as the radiation source of wavelength = 1.5406 Å at 40 kV, 40 mA, and at room temperature conditions. The scan speed was set to be 0.5/min over 10°–90° scan range.

Carl Zeiss FE-SEM Sigma VP-03-67, with operating conditions of 20 kV over the working distance of 6–9 mm, was used to study the morphological characteristics of the catalysts. All the samples were ground into a fine powder with a mortar and pestle prior to the analysis. The analysis was completed by placing a small amount of the powdered sample to a piece of two-way carbon tape and mounted to a sample holder (stub). The elemental composition of the sample was carried out on an Oxford instruments X-MaxN 50 model 54-XMX1003 EDX analyser.

TEM analysis was conducted using a JOEL JEM-1010 transmission electron microscope with an acceleration voltage of 100 kV. The images were captured with a Meagaview III camera and analysed

with iTEM imaging software. The sample preparation involved dispersing the powdered samples into toluene for 20 min. The analysis was conducted by placing a drop of the catalyst sample on a copper grid coated with formvar with a mesh size of 150 and allowing it to dry at room temperature before the TEM images were captured.

An Agilent 700 series ICP-OES with a 710 ICP-OES detector instrument was used to quantify manganese content from the Mn loaded γ-Al_2O_3 catalysts. A series of standard solutions were prepared from manganese chloride tetrahydrate. The samples were prepared by digestion of 0.15 g of the 2.5%, 5%, 7.5%, 10%, 12.5%, and 15% Mn/γ-Al_2O_3 catalysts in a mixture of 3 mL HCl, 3 mL HNO_3, and 4 mL HF at 60 °C for 1 h until digestion was complete. The sample preparation was completed by subsequent dilution of the resultant solution with distilled water up to the 100 mL mark of the volumetric flask to make 25, 50, 75, 100, 125, and 150 ppm for 2.5%, 7.5%, 5%, 10%, 12.5%, and 15% Mn/γ-Al_2O_3 catalysts, respectively.

The surface areas of the catalysts were analysed with Brunauer-Emmet-Teller (BET) surface area analyser. Prior to the analysis, the catalysts were degassed at 250 °C for 12 h under N_2 flow in micrometrics flow prep 060. Subsequently, the catalysts were analysed in an automated single, and then multiple, point micrometrics Gemini 2360 BET surface area analyser under nitrogen flow.

3.3. Oxidation of Cyclohexane

The oxidation of cyclohexane was carried out in an impinger reactor with a porous bubbler. The substrate (cyclohexane) was added into the reaction vessel. The ozone was fed into the reaction vessel through the porous bubbler. Initially, cyclohexane ozonation was studied in a catalyst-free system. Subsequently, ozonation reaction was catalysed with bear γ-Al_2O_3 and various percentages of Mn/γ-Al_2O_3 catalysts. All ozonation reactions were studied at pH 3, 7, and 11. Aqueous solutions of acetic acid (0.1 M) and sodium hydroxide (0.1 M) were used to adjust pH. Two solutions resulted upon the acetic and hydroxide addition. A total of 50 mL of cyclohexane and 0.2 g of the catalysts were used in all oxidation reactions. The pH of the reaction mixture increased from pH = 7.1 to pH = 7.9 upon addition of the catalysts. Acetic acid was used to obtain pH = 7. The typical cyclohexane oxidation setup is shown in Figure 9.

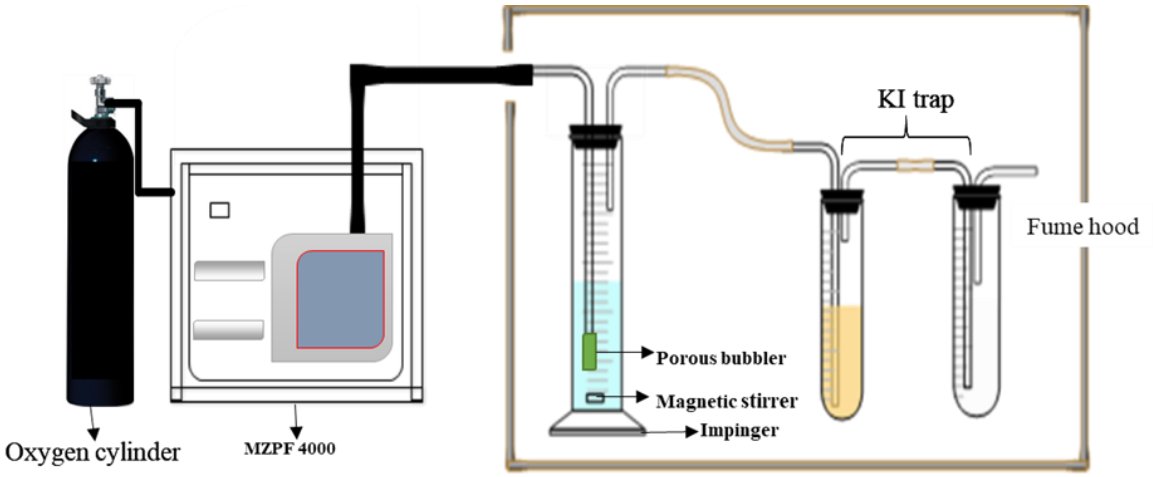

Figure 9. The typical reaction setup for the cyclohexane ozonation.

3.4. Reaction Products Characterisation

Fourier transform infrared spectroscopy: The typical FT-IR spectroscopy, as discussed in Section 2.2 for the analysis of catalysts, was also used to analyse the reaction products. However, the pressure applied for proper contact between the sample and the sample holder was not adjusted to 90 gauge because the reaction products were in liquid form with low viscosity.

Gas Chromatography-Mass Spectroscopy (GC-MS)

The gas chromatography-mass spectroscopy analyses were conducted using an Agilent 7890A gas chromatograph and helium as a carrier gas at a flow rate of 0.7 mL/min and Agilent HP-5MS, 5% phenyl methyl siloxane column with column dimensions of 30 m × 250 μm × 0.25 μm. The gas chromatograph was coupled with a 5975VL mass selective detector (MSD). The initial oven temperature was 60 °C, and it was kept constant for 2 min and then ramped up to a final temperature of 280 °C at a rate of 10 °C/min. A total of 2 μL of the sample was injected manually through the column inlet using a microsyringe.

4. Conclusions

The catalytic effect of the Mn/γ-Al_2O_3 catalysts has been evaluated for selective oxidation of cyclohaxane at 20 °C and 1 atm of temperature and pressure conditions, respectively. It has been demonstrated that the Mn/γ-Al_2O_3 catalysts are highly active and selective for the oxidation of cyclohexane to KA oil. The optimisation of the reaction time from 30 min to 1 h and pH 3, 7, and 11 increased the percentage conversion of cyclohexane without compromising the selectivity. The increase in the percentage of the Mn loading onto γ-Al_2O_3 from 2.5% to 15% is accompanied by a decrease in percentage conversion of cyclohexane. However, the selectivity to KA oil and/or cyclohexanone is not compromised. The results indicate that the 2.5% Mn/γ-Al_2O_3 catalyst exhibit better catalytic performance with cyclohexane percentage conversion of 13% at pH 3, 16% at pH 7, and 23% at pH 11 after 30 min of ozonation time. The selectivity is 100% toward KA oil. After 1 h of ozonation time, the percentage conversion of cyclohexane is 23 at pH 3, 29 at pH 7, and 36 at pH 11. The percentage selectivity at pH 3 and 7 is 100% toward cyclohexanone. Nevertheless, at pH 11, the mixture of cyclohexanol and cyclohexanone (KA oil) is obtained. From the reaction products obtained, it can be concluded that cyclohexane is first oxidised to cyclohexanol, which is further oxidised to cyclohexanone. Furthermore, the increase in pH is accompanied by an increase in radical production from the decomposition of ozone, which provided better oxidation potential than ozone, hence the observed increase in cyclohexane percentage conversion at pH 11. Lastly, the use of ambient temperature and pressure conditions (20 °C and 1 atm) plays a crucial role in optimising the percentage selectivity towards KA oil. In conclusion, the Mn/γ-Al_2O_3 catalyst presents great potential as the industrial catalyst for the oxidation of cyclohexane at ambient temperature and pressure.

Supplementary Materials: The following are available online at http://www.mdpi.com/2073-4344/9/11/958/s1, Figure S1: SEM images of (a) 10% Mn/γ-Al_2O_3, (b) 12.5% Mn/γ-Al_2O_3, and (c) 15% Mn/γ-Al_2O_3 catalysts.; Figure S2: TEM images of (a) 10% Mn/γ-Al_2O_3, (b) 12.5% Mn/γ-Al_2O_3, and (c) 15% Mn/γ-Al_2O_3 catalysts.; Figure S3 (a): SEM-EDX image for 2.5% Mn/γ-Al_2O_3 catalyst.; Figure S3 (b): SEM-EDX image for 5 % Mn/γ-Al_2O_3 catalyst.; Figure S3 (c): SEM-EDX image for 7.5 % Mn/γ-Al_2O_3 catalyst.; Figure S3 (d): SEM-EDX image for 10% Mn/γ-Al_2O_3 catalyst.; Figure S3 (e): SEM-EDX image for 12.5 % Mn/γ-Al_2O_3 catalyst.; Figure S3 (f): SEM-EDX image for 15% Mn/γ-Al_2O_3 catalyst.; Figure S4: (a) Gas chromatogram and (b) mass spectrum of cyclohexane before ozonation.; Figure S5: (a) Gas chromatogram and mass spectra of (b) cyclohexane, (c) cyclohexanol, and (d) cyclohexanone after 30 minutes of ozonation.; Figure S6: (a) Gas chromatogram and mass spectra of (b) cyclohexane and (c) cyclohexanone after 1 h of ozonation.

Author Contributions: Conceptualisation, V.S.R.P.; methodology, V.S.R.P.; formal analysis, S.T.M. and V.S.R.P.; investigation, S.T.M. and V.S.R.P.; writing—original draft preparation, S.T.M. and V.S.R.P.; writing—review and editing, V.S.R.P.; supervision, V.S.R.P.; project administration, V.S.R.P.; funding acquisition, V.S.R.P.

Funding: Rajasekhar Pullabhotla would like to acknowledge the Research and Innovation Office, UZ, for the financial support in the form of Project S 451/12 and National Research Foundation (NRF, South Arica) for the financial support in the form of the Incentive Fund Grant (Grant No: 103691) and Research Developmental Grant for Rated Researchers (112145).

Acknowledgments: The authors acknowledge the EMU at the University of KwaZulu-Natal, Westville campus, for providing us access to their TEM facility. Rajasekhar Pullabhotla would like to acknowledge the Research and Innovation Office, UZ, for the financial support in the form of Project S 451/12 and the National Research Foundation (NRF, South Arica) for the financial support in the form of the Incentive Fund Grant (Grant No: 103691).

Conflicts of Interest: The authors declare no conflict of interest.

References

1. Son, L.; Liu, J.; Lou, W.; Yang, Y.; Wang, F.; Weerakkody, C.; Suib, S.L. Preparation of amorphous copper-chromium oxides catalyst for selective oxidation of cyclohexane. *Mol. Catal.* **2018**, *460*, 16–26. [CrossRef]
2. Xu, L.X.; He, C.H.; Zhu, M.Q.; Fang, S. A highly active Au/Al_2O_3 catalyst for cyclohexane oxidation using molecular oxygen. *Catal. Lett.* **2007**, *114*, 202–205. [CrossRef]
3. Savita, K.; Priti, S. Solvent-free oxidation of cyclohexane over covalently anchored transition-metal salicylaldimine complexes to α-zirconium phosphate using tert-butylhydroperoxide. *J. Mol. Catal. A* **2016**, *411*, 279–289.
4. Zhou, L.; Xu, J.; Miao, H.; Wang, F.; Li, X. Catalytic oxidation of cyclohexane to cyclohexanol and cyclohexanone over Co_3O_4 nanocrystals with molecular oxygen. *Appl. Catal.* **2005**, *292*, 223–228. [CrossRef]
5. Unnarkat, A.P.; Sridhar, T.; Wang, H.; Mahajani, S.; Suresh, A.K. Cobalt molebdenum oxide catalysts for selective oxidation of cyclohexane. *React. Eng. Kinet. Catal.* **2016**, *62*, 4384–4402.
6. Raja, R.; Ratnasamy, P. Oxidation of cyclohexane over copper phthalocyanines encapsulated in zeolites. *Catal. Lett.* **1997**, *48*, 1–10. [CrossRef]
7. Fu, Y.; Zhan, W.; Guo, Y.; Wang, Y.; Liu, X.; Guo, Y.; Wang, Y.; Lu, G. Effect of surface functionalization of cerium-doped MCM-48 on its catalytic performance for liquid-phase free solvent oxidation of cyclohexane with molecular oxygen. *Microporous Mesoporous Mater.* **2015**, *214*, 101–107. [CrossRef]
8. Venart, J.E.S. The explosion and its aftermaths. *Process Saf. Environ. Prot.* **2004**, *82*, 105–127. [CrossRef]
9. Sadie, C.; Samuels, D.E.; Obrien, T.P. The characteristics of the explosion of cyclohexane at the Nypro (UK) Flixborough plant on 1st June 1974. *J. Occup. Accid.* **1977**, *1*, 203–235. [CrossRef]
10. Bose, P.; Glaze, W.H.; Maddox, D.S. Degradation of various advanced oxidation processes: 1. Reaction rates. *Water Res.* **1998**, *23*, 997–1004. [CrossRef]
11. Wang, H.C.; Liang, H.S.; Chang, M.B. Oxidation of chlorobenzene using ozone over iron oxide and manganese oxide catalysts. *J. Hazard. Mater.* **2011**, *186*, 1781–1787. [CrossRef] [PubMed]
12. Walling, C. Fenton's reagent revisited. *Acc. Chem. Res.* **1975**, *8*, 125–131. [CrossRef]
13. Suh, J.H.; Mohsu, M. A study of relationship between biodegradability enhancement and oxidation of 1, 4-dioxane using ozone and hydrogen peroxide. *Water Res.* **2014**, *126*, 92–96. [CrossRef] [PubMed]
14. Ollis, D.F.; Pelizzetti, E.; Serpone, N. Photocatalyzed destruction of water contaminants. *Environ. Sci. Technol.* **1991**, *25*, 1523–1529. [CrossRef]
15. Masten, S.J.; Davies, S.H. The use of ozonation to degrade organic contaminants in wastewaters. *Environ. Sci. Technol.* **1994**, *28*, 180–185. [CrossRef]
16. Pullabhotla, V.S.R.R.; Jonnalagadda, S.B. Scope of Metal Loaded Microporous ZSM-5 Zeolites in the "Catazone" Process of n-Hexadecane at Moderate Conditions. *Ind. Eng. Chem. Res.* **2009**, *48*, 9097–9105. [CrossRef]
17. Pegis, M.L.; Roberts, J.A.S.; Wasylenko, D.J.; Mader, E.A.; Appel, A.M.; Mayer, J.M. Standard Reduction Potentials for Oxygen and Carbon Dioxide Couples in Acetonitrile and N,N-Dimethylformamide. *Inorg. Chem.* **2015**, *54*, 11883–11888. [CrossRef]
18. Forni, L.; Behnemann, D.; Hart, E.J. Mechanism of the hydroxide ion initiated decomposition of ozone in aqueous solution. *J. Phys. Chem.* **1982**, *86*, 255–259. [CrossRef]
19. Li, W.; Oyama, S.T. Mechanism of Ozone Decomposition on a Manganese Oxide Catalyst. 2. Steady-State and Transient Kinetic Studies. *J. Am. Chem. Soc.* **1998**, *35*, 9047–9052. [CrossRef]
20. Nelieu, S.; Kerhoas, L.; Einhorn, J. Degradation of atrazine into ammeline by combined ozone/hydrogen peroxide treatment in water. *Environ. Sci. Technol.* **2000**, *34*, 430–437. [CrossRef]
21. McGrane, W. Advanced oxidation processes for destruction and enhanced biodegradability of 1,4-dioxane. *Chem. Oxid.* **1997**, *6*, 231–245.
22. Beltran, F.; Acedo, B.; Rivas, J. Use of ozone and hydrogen peroxide to remove alachlor from surface water. *Bull. Environ. Contam. Toxicol. J.* **1999**, *63*, 9–14. [CrossRef] [PubMed]
23. Gulyas, H.; von Bismarck, R.; Hemmerling, L. Treatment of industrial wastewaters with ozone/hydrogen peroxide. *Water Sci. Technol.* **1995**, *7*, 127–134. [CrossRef]

24. Wu, H.; Pantaleo, G.; Venezia, A.M.; Liotta, L.F. Mesoporous Silica Based Gold Catalysts: Novel Synthesis and Application in Catalytic Oxidation of CO and Volatile Organic Compounds (VOCs). *Catalysts* **2013**, *3*, 774–793. [CrossRef]
25. Lan, S.; Guo, N.; Gan, S. Facile preparation of hierarchical hollow structure gamma alumina and study of its adsorption capacity. *Appl. Catal.* **2012**, *97*, 83–90. [CrossRef]
26. Karim, M.R.; Rahman, M.A.; Ito, M. synthesis of gamma alumina catalysts and surface characterisation. *Open Colloid Sci. J.* **2011**, *4*, 32–36. [CrossRef]
27. Ncanana, Z.S.; Pullabhotla, V.S.R.R. Ozone Initiated Oxidation of Cresol Isomers Using γ-Al_2O_3 and SiO_2 as Adsorbents. *Catal. Lett.* **2018**, *148*, 1535–1546. [CrossRef]
28. Maldonado, C.; Lucio-Ortiz, C.J.; De la Rosa, J.R.; Ramírez, A.H. Synthesis and characterization of Fe doped mesoporous Al_2O_3 by sol–Gel method and its use in trichloroethylene combustion. *J. Sol Gel Sci. Technol.* **2011**, *58*, 374–384.
29. Syroezhko, A.M.; Begak, O.Y.; Proskuryakov, V.P. Catalytic Oxidation of Cyclohexane with Ozone-Oxygen Mixtures. *Russ. J. Appl. Chem.* **2004**, *77*, 51–56. [CrossRef]
30. Liang, S.; Hao, C.; Shi, Y. The Power of Single-Atom Catalysis. *ChemCatChem* **2015**, *7*, 2559–2567. [CrossRef]
31. Nguyen, T.Q.; Escaño, M.C.S.; Nakanishi, H.; Kasai, H.; Maekawa, H.; Osumi, K.; Sato, K. DFT+ U study on the oxygen adsorption and dissociation on CeO_2-supported platinum cluster. *Appl. Surf. Sci.* **2014**, *288*, 244–250. [CrossRef]
32. Védrine, J.C. Heterogeneous Catalysis on Metal Oxides. *Catalysts* **2017**, *7*, 341.
33. Ross, J.R.H. *Heterogeneous Catalysis*; Elsevier: Amsterdam, The Netherlands, 2012; pp. 47–64.
34. Conte, M.; Liu, X.; Murphy, D.M.; Whiston, K.; Hutchings, G.J. Cyclohexane oxidation using Au/MgO: An investigation of the reaction mechanism. *Phys. Chem. Chem. Phys.* **2012**, *14*, 16279–16285. [CrossRef] [PubMed]
35. Kruanak, K.; Jarusutthirak, C. Degradation of 2,4,6-trichlorophenol in synthetic wastewater by catalytic 450 ozonation using alumina supported nickel oxides. *J. Environ. Chem. Eng.* **2019**, *7*, 102825. [CrossRef]
36. Pullabhotla, V.S.R.R.; Jonnalagadda, S.B. Scope of Metal Loaded Microporous Zeolite-Y as Catalyst in Ozone Initiated Oxidation of n-hexadecane. *J. Adv. Oxid. Technol.* **2009**, *12*, 179–187. [CrossRef]
37. Pullabhotla, V.S.R.R.; Rahman, A.; Jonnalagadda, S.B. Selective catalytic Knoevenagel condensation by Ni-SiO_2 supported heterogeneous catalysts: An environmental benign approach. *Catal. Commun.* **2009**, *10*, 365–369.